buildings

MDPI

Article

A Multi-Source Fusion Deformation Monitoring Method for Super High-Rise Buildings Based on WOA-VMD and Adaptive Robust Kalman Filtering

Liangliang Yang [1], Jian Wang [1,*], Yulong Jiang [2], Pengfei Wang [1], Ping Zhu [1] and Yilong Yu [2]

[1] School of Geomatics and Urban Spatial Informatics, Beijing University of Civil Engineering and Architecture, Beijing 102616, China; 1108160025013@stu.bucea.edu.cn (L.Y.)
[2] China State Construction Hongda Engineering Co., Ltd., Beijing 100125, China
* Correspondence: wangjian@bucea.edu.cn

Abstract

Super high-rise buildings are increasingly equipped with structural monitoring systems to track deformation responses during construction and operation, thereby supporting structural condition assessment and engineering management. To address key monitoring challenges, including GNSS multipath interference, insufficient vertical accuracy, accelerometer integration drift, and high-frequency noise, this study proposes a GNSS/accelerometer fusion monitoring method based on whale optimization algorithm–optimized variational mode decomposition (WOA-VMD) and adaptive robust Kalman filtering (ARKF). Continuous three-hour GNSS and accelerometer observations collected from a super high-rise building under construction are used for fusion validation. The results show that WOA-VMD effectively separates noise from deformation-related signals and outperforms conventional EMD and standard VMD in denoising performance. Compared with the raw observations, the fused east, north, and vertical displacement RMSEs are reduced by 68.84%, 75.97%, and 60.22%, respectively; the SNRs increase to 22.03 dB, 21.38 dB, and 16.74 dB, respectively; the STDs decrease by 72.58%, 75.62%, and 68.39%, respectively; and the PSDs increase to 9.47 dB, 9.02 dB, and 8.31 dB, respectively. The proposed framework exhibits sub-centimeter-level displacement monitoring performance in the horizontal directions and significantly enhances the monitoring capability of the vertical component. The field validation results demonstrate the feasibility and effectiveness of the proposed framework for short-term deformation monitoring of super high-rise buildings under practical monitoring conditions and indicate its potential for structural health monitoring applications.

Keywords: super high-rise building; deformation monitoring; WOA-VMD; multi-source data fusion

Check for updates

Academic Editor: Antonio Caggiano

Received: 14 May 2026
Revised: 22 June 2026
Accepted: 22 June 2026
Published: 24 June 2026

Copyright: © 2026 by the authors. Licensee MDPI, Basel, Switzerland. This article is an open access article distributed under the terms and conditions of the Creative Commons Attribution (CC BY) license.

1. Introduction

Super-tall buildings are important components of modern urban infrastructure and are increasingly employed to accommodate intensive land use and multifunctional urban development [1]. During construction and service periods, these structures are continuously subjected to wind loads, temperature variations, long-term gravity effects, differential settlement, and construction disturbances, which may induce cumulative deformation and dynamic responses [2]. Accurate monitoring of structural deformation is therefore essential for assessing structural condition, identifying abnormal behavior, and supporting safe operation and maintenance [3].

Against this background, many scholars have carried out extensive frontier research. Wang et al. [4] systematically reviewed the technical framework of GNSS multi-source fusion for super high-rise building deformation monitoring, summarizing the method system from the perspectives of signal processing, multi-sensor integration, and filtering algorithms, thereby providing theoretical guidance for collaborative multi-source monitoring. Bao et al. [5] combined GNSS with accelerometers and used multi-rate filtering and smoothing strategies to extract dynamic deformation, confirming the advantages of multi-sensor complementarity in improving the characterization of high-frequency responses. Huang et al. [6] combined GNSS with a robotic total station to effectively weaken the influence of instantaneous vibration on intermediate-floor monitoring in super-tall buildings and improve the stability of displacement observations. Hayat et al. [7] comprehensively reviewed mainstream sensing technologies, deployment strategies, and energy supply solutions in structural health monitoring, providing references for the selection and deployment of super high-rise monitoring systems. Since large-scale projects such as Canary Wharf Tower first introduced satellite positioning into structural dynamic monitoring, GNSS has gradually become a core means of long-term deformation monitoring for super high-rise buildings because of its continuous observation, three-dimensional positioning, and no requirement for intervisibility. Shen et al. [8] revealed the potential and limitations of GNSS in structural health monitoring from the perspectives of multi-constellation fusion, sensor integration, and algorithmic denoising, promoting the development of dynamic monitoring technologies toward lower cost, wider coverage, and higher precision.

At present, safety monitoring of super high-rise buildings is shifting from conventional periodic inspection toward real-time, intelligent, and preventive monitoring. Its core objective is to achieve early identification, early warning, and early response through continuous dynamic sensing, thereby minimizing operation and maintenance costs and reducing the risk of structural damage [9]. This transition imposes stringent requirements on monitoring technologies: the system must simultaneously capture millimeter-level micro-deformation, high-frequency vibration under strong wind, and long-term slow settlement, while maintaining stable and reliable performance in complex urban environments. In this context, the fusion of GNSS and inertial sensing has gradually become a mainstream technical route for dynamic deformation sensing of super high-rise buildings [10].

In practical engineering applications, GNSS can directly obtain three-dimensional absolute displacement and has the advantages of all-weather operation and long-term stability. It is therefore widely used for monitoring low-frequency settlement and overall sway of super high-rise buildings [11]. However, most super high-rise buildings are located in dense urban areas, where building reflections, signal blockage, and low-elevation satellite signals can cause significant multipath effects. Together with relatively low sampling rates, these factors restrict vertical accuracy and lead to the loss of high-frequency information, making it difficult to satisfy the monitoring requirements of wind-induced vibration and other dynamic responses [12]. As a complementary sensor, accelerometers provide high sampling rates and high dynamic sensitivity, enabling accurate capture of instantaneous structural vibration and high-frequency responses. Nevertheless, their signals are vulnerable to temperature drift, bias errors, and high-frequency noise, and the errors accumulate rapidly during double integration. As a result, severe drift occurs when accelerometers are used independently for long periods, and reliable absolute displacement cannot be obtained directly [13,14]. Existing studies mainly focus on single-sensor denoising or hardware improvement, while insufficient attention has been paid to efficient collaborative mechanisms for multi-source information. In recent years, advanced machine-learning and data-driven approaches have also been introduced into structural monitoring, signal processing, and predictive modeling. Representative exam-

ples include the High Correlated Variable Creator Machine (HCVCM) and the Stronger Variable Creator Machine (SVCM), which have demonstrated promising capabilities in nonlinear feature construction, variable generation, and prediction enhancement under complex data conditions [15,16]. Although these methods provide valuable insights for intelligent data analysis, their application in GNSS/accelerometer collaborative deformation monitoring of super high-rise buildings remains limited. Consequently, developing a robust physics-guided and multi-sensor fusion framework capable of accommodating heterogeneous observations and complex noise environments continues to be an important research challenge.

To address the critical challenges encountered in dynamic deformation monitoring of super-tall buildings, including severe Global Navigation Satellite System (GNSS) multipath effects, insufficient vertical positioning performance, significant accelerometer integration drift, and high-frequency measurement noise, this study proposes a GNSS/accelerometer fusion framework based on the Whale Optimization Algorithm (WOA), Variational Mode Decomposition (VMD), and Adaptive Robust Kalman Filtering (ARKF). First, considering the distinct error characteristics of GNSS and accelerometer observations, a differentiated signal preprocessing strategy is developed, in which dedicated VMD reconstruction rules are designed for each sensor type rather than employing a unified denoising scheme. This strategy effectively suppresses GNSS multipath errors, accelerometer low-frequency drift, and high-frequency measurement noise, thereby improving the consistency and reliability of heterogeneous observations prior to data fusion. Second, a hierarchical WOA–VMD–ARKF collaborative fusion architecture is established for deformation monitoring of super-tall buildings. In this framework, WOA is employed to adaptively optimize the key VMD parameters, enabling signal-domain enhancement, while ARKF performs robust multi-rate data fusion under non-Gaussian and time-varying noise conditions, thereby achieving improved state estimation performance. Consequently, a two-level optimization mechanism integrating signal-domain enhancement and state-domain estimation is realized. Finally, the proposed framework is systematically evaluated using both numerical simulations and field monitoring data collected from an under-construction super-tall building. The results demonstrate that the proposed method effectively mitigates the adverse effects of GNSS multipath interference, accelerometer drift, and complex environmental disturbances, while enhancing the consistency and reliability of multi-source deformation observations. The field experiments further verify the feasibility and effectiveness of the proposed framework for short-term deformation monitoring under practical engineering conditions. The developed framework provides a promising solution for structural deformation monitoring and dynamic response identification of super-tall buildings and demonstrates potential for future structural health monitoring applications.

2. Core Algorithm Principles

2.1. Variational Mode Decomposition

Variational mode decomposition (VMD), proposed by Dragomiretskiy and Zosso, is an adaptive variational decomposition method for non-stationary signals [17]. From a frequency-domain perspective, VMD models non-stationary signals by explicitly constraining modal bandwidths and center frequencies, thereby enabling stable separation of signal components at different scales. Compared with empirical mode decomposition (EMD) and its improved variants, VMD does not rely on recursive sifting. It has a well-defined mathematical optimization model and good numerical stability, and it shows clear advantages in suppressing mode mixing and noise interference. It is there-

fore particularly suitable for nonlinear and non-stationary signal processing in complex engineering environments [18–20].

The basic assumption of VMD is that an input signal $f(t)$ can be represented as several modal components with finite bandwidths and different center frequencies u_k ($k = 1, 2, \ldots, K$). Each modal component is concentrated around its corresponding center frequency in the frequency domain, and its bandwidth can be measured by the L_2 norm of the gradient after modulation to the baseband. On this basis, VMD constructs a constrained variational problem that minimizes the sum of modal bandwidths under the condition that the sum of all modes equals the original signal, thereby achieving optimal signal decomposition. The variational model is formulated as Equation (1):

$$\begin{cases} \min\limits_{\{u_k\},\{\omega_k\}} \left(\sum \left\| \partial_t \left[\left(\delta(t) + \frac{j}{\pi t} \right) * u_k(t) \right] e^{-j\omega_k t} \right\|_2^2 \right) \\ \text{s.t.} \sum\limits_k u_k = f(t) \end{cases}. \tag{1}$$

where u_k denotes the k-th modal component, ω_k is the corresponding center frequency, K is the preset number of modes, and * denotes the convolution operation.

To solve the above constrained optimization problem, VMD introduces a quadratic penalty term and a Lagrange multiplier to transform it into an unconstrained optimization model, as shown in Equation (2). The penalty factor α is used to balance the reconstruction error and modal bandwidth constraints, while the Lagrange multiplier λ is used to ensure the approximation accuracy of the sum of modal components to the original signal. The model is solved in the frequency domain using the alternating direction method of multipliers (ADMM). During each iteration, the modal components, center frequencies, and Lagrange multiplier are updated alternately until the optimal solution is approached:

$$\begin{aligned} L(\{u_k\},\{\omega_k\},\lambda) = \alpha \sum_k \left\| \partial_t \left[\left(\delta(t) + \frac{j}{\pi t} \right) * u_k(t) \right] e^{-j\omega_k t} \right\|_2^2 \\ + \left\| f(t) - \sum_k u_k(t) \right\|_2^2 + \left[\lambda(t), f(t) - \sum_k u_k(t) \right] \end{aligned}, \tag{2}$$

$$\hat{u}_k^{n+1}(\omega) = \frac{\hat{f}(\omega) - \sum\limits_{i<k} \hat{u}_i^{n+1}(\omega) - \sum\limits_{i>k} \hat{u}_i^{n}(\omega) + \frac{\hat{\lambda}^n(\omega)}{2}}{1 + 2\alpha(\omega - \omega_k^n)^2}, \tag{3}$$

$$\omega_k^{n+1} = \frac{\int_0^\infty \omega \left| \hat{u}_k^{n+1}(\omega) \right|^2 d\omega}{\int_0^\infty \left| \hat{u}_k^{n+1}(\omega) \right|^2 d\omega}, \tag{4}$$

Specifically, in the $(n+1)$-th iteration, the frequency-domain expression of each modal component is updated according to Equation (3). The update process is essentially equivalent to performing adaptive bandpass filtering on the signal spectrum, with the center of the passband determined by the center frequency ω_k^n of the current iteration step. The center frequency is then corrected according to Equation (4) by calculating the energy-weighted average of the updated modal component in the frequency domain, so that it gradually converges to the dominant frequency of the corresponding mode. The Lagrange multiplier is updated through residual feedback to ensure the completeness and convergence stability of modal reconstruction [21,22].

To achieve precise screening of effective modes, this paper constructs a dual-threshold screening criterion based on the modal center frequency and energy proportion. Define the energy of the k-th modal component as E_k and η_k as follows:

$$E_k = \sum |u_k(t)|^2,\ \eta_k = \frac{E_k}{\sum_{k=1}^{K} E_k}, \tag{5}$$

When the modal center frequency f_k is lower than 0.1 Hz or higher than 10 Hz, the mode is regarded as a trend term or a high-frequency noise component and is removed. At the same time, only modes with an energy proportion greater than 5% are retained for signal reconstruction. This strategy maximally preserves deformation features while accurately filtering noise, thereby improving the stability and repeatability of signal denoising.

2.2. Whale Optimization Algorithm

Although VMD has strong theoretical signal decomposition capability, its performance depends heavily on the number of modes K and the penalty parameter. An excessively large K may lead to over-decomposition and spectral mixing, whereas an excessively small K may cause under-decomposition, in which multiple signal components are merged into one mode. An overly large penalty parameter may impose an excessively narrow bandwidth constraint and cause the loss of useful frequency-band information, whereas an overly small value may retain redundant components and weaken the denoising effect. Therefore, K and the penalty parameter must be adaptively optimized to ensure the decomposition performance of VMD.

The whale optimization algorithm (WOA), proposed by Mirjalili and Lewis, is a population-intelligence-based continuous optimization method [23]. It is inspired by the cooperative behavior and bubble-net hunting mechanism of humpback whales during predation. WOA maps the solution space of an optimization problem to a search environment, treats each candidate solution as an individual whale, and approaches the global optimum through cooperative iterative search. Compared with traditional intelligent optimization algorithms, WOA has a simple structure, few parameters, and low implementation cost, and it has been widely applied in engineering optimization, parameter identification, and signal processing.

The search mechanism of the Whale Optimization Algorithm (WOA) mainly consists of three types of behaviors: prey encircling, bubble-net attacking, and random searching.

In the prey encircling phase, the algorithm assumes that the current global optimal solution corresponds to the prey location, and other individuals gradually converge toward the optimal solution under the modulation of the coefficient vector. The distance vector and coefficient vector are first defined as follows:

$$\boldsymbol{D} = |\boldsymbol{C} \cdot \boldsymbol{X}^*(t) - \boldsymbol{X}(t)|, \tag{6}$$

$$\boldsymbol{X}(t+1) = \boldsymbol{X}^*(t) - \boldsymbol{A} \cdot \boldsymbol{D}, \tag{7}$$

where t denotes the current iteration number, $\boldsymbol{X}^*(t)$ represents the position of the current optimal individual, $\boldsymbol{X}(t)$ stands for the current position of a whale, and $\boldsymbol{A}$ and $\boldsymbol{C}$ are the control coefficient vectors that satisfy:

$$\boldsymbol{A} = 2\boldsymbol{a} \cdot \boldsymbol{r} - \boldsymbol{a},\ \boldsymbol{C} = 2\boldsymbol{r}, \tag{8}$$

$\boldsymbol{r}$ is a random vector uniformly distributed over [0, 1], and the convergence factor $\boldsymbol{a}$ decreases linearly with the number of iterations.

$$\boldsymbol{a} = 2 - \frac{2t}{T_{\max}}, \tag{9}$$

In the bubble-net attacking phase, the algorithm switches between the shrinking encircling mechanism and the spiral updating strategy in a probabilistic manner to simulate the predation trajectory of humpback whales spiraling around prey, thereby enhancing the local search capability.

$$\boldsymbol{X}(t+1) = \boldsymbol{D} \cdot e^{bl} \cdot \cos(2\pi l) + \boldsymbol{X}^*(t), \tag{10}$$

where b is a constant for defining the spiral shape, $l \in [-1, 1]$ is a random number, and the algorithm adaptively switches between shrinking the encircling mechanism and spiral updating with a probability $p \in [0, 1]$.

$$\boldsymbol{X}(t+1) = \begin{cases} \boldsymbol{X}^*(t) - \boldsymbol{A} \cdot \boldsymbol{D}, & p < 0.5 \\ \boldsymbol{D} \cdot e^{bl} \cos(2\pi l) + \boldsymbol{X}^*(t), & p \geq 0.5 \end{cases}, \tag{11}$$

When the amplitude of the coefficient vector is large, the algorithm enters the random search phase, where each whale updates its position with reference to a random individual to expand the search range and avoid premature convergence.

When $|\boldsymbol{A}| \geq 1$, the algorithm abandons the current optimal solution and performs global search with reference to a random individual $\boldsymbol{X}_{\text{rand}}(t)$.

$$\boldsymbol{D} = |\boldsymbol{C} \cdot \boldsymbol{X}_{\text{rand}}(t) - \boldsymbol{X}(t)|, \tag{12}$$

$$\boldsymbol{X}(t+1) = \boldsymbol{X}_{\text{rand}}(t) - \boldsymbol{A} \cdot \boldsymbol{D}, \tag{13}$$

Therein, the convergence factor decreases linearly with the iteration process, enabling the algorithm to achieve a smooth transition between global exploration and local exploitation [24–27].

With the above mechanisms, WOA can achieve adaptive adjustment of search strategies with fewer control parameters, balancing the ergodicity of the solution space and convergence accuracy. However, in high-dimensional, strong-noise or multi-modal optimization problems, the original WOA still suffers from insufficient convergence speed and the risk of falling into local optima. Therefore, in recent years, most related studies have improved its performance by introducing modified search paths, adaptive parameter adjustment, hybrid perturbation mechanisms, and so on. Due to its good engineering applicability and parameter optimization capability, WOA provides an effective global search tool for complex signal processing and model parameter optimization problems [28] (Figure 1).

2.3. Adaptive Robust Kalman Filter

The classical Kalman filter (KF) can provide linear unbiased optimal estimation under the ideal assumptions that process noise and measurement noise follow zero-mean Gaussian distributions and that their statistical characteristics are known. However, in practical engineering scenarios such as super high-rise building deformation monitoring, urban multipath interference, sensor anomalies, and sudden environmental disturbances may cause observation noise to become non-Gaussian, non-stationary, and contaminated by outliers. This can lead to mismatched filtering gains, reduced estimation accuracy, and even divergence in the conventional KF. Therefore, this study constructs an adaptive robust Kalman filter (ARKF) that integrates robust estimation with adaptive noise correction

to suppress the influence of abnormal observations, adapt online to time-varying noise characteristics, and improve the stability and reliability of multi-source data fusion [29–32].

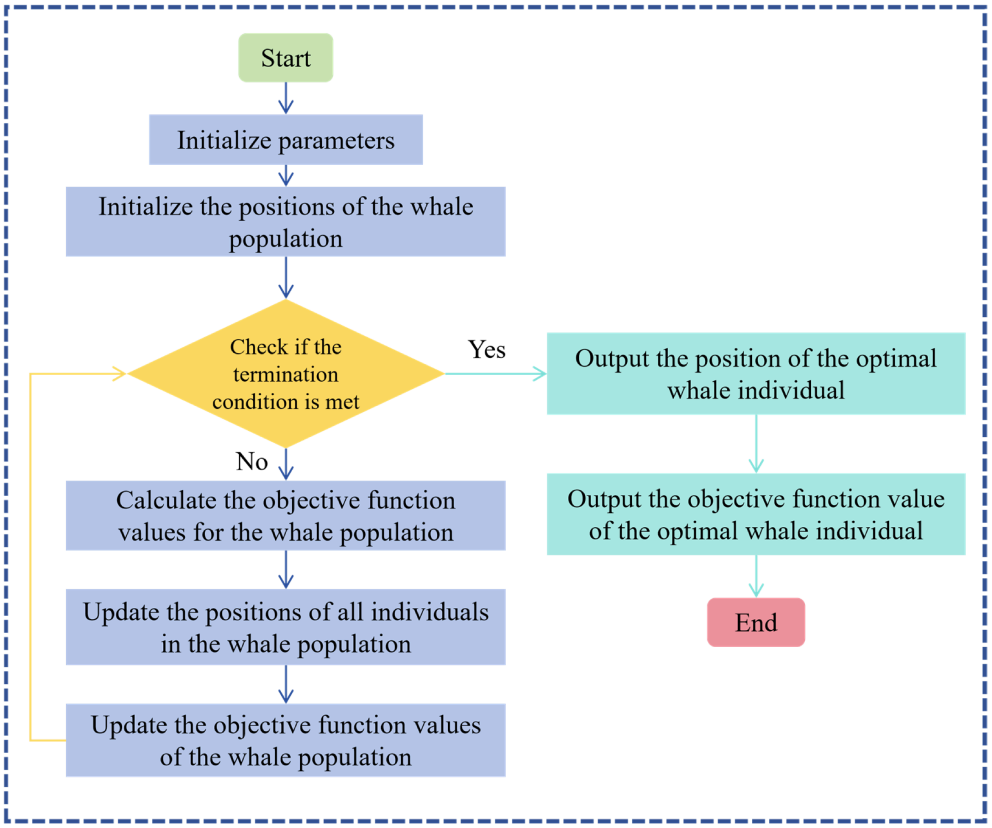


Figure 1. Flowchart of the WOA.

In the classical Kalman filtering framework, the system state and observation models are usually expressed as follows:

$$\begin{aligned} \mathbf{x}_k &= \mathbf{F}_{k-1}\mathbf{x}_{k-1} + \mathbf{w}_{k-1} \\ \mathbf{z}_k &= \mathbf{H}_k\mathbf{x}_k + \mathbf{v}_k \end{aligned}, \tag{14}$$

where $\mathbf{x}_k$ denotes the system state vector, $\mathbf{z}_k$ denotes the observation vector, and $\mathbf{w}_{k-1}$ and $\mathbf{v}_k$ denote the process noise and measurement noise, respectively, which are generally assumed to follow zero-mean Gaussian distributions. In complex engineering environments, however, sensor anomalies, signal blockage, and abrupt disturbances can make measurement noise non-Gaussian, under which the conventional KF is prone to filtering divergence or estimation bias.

The robust Kalman filter (RKF) introduces robust statistical concepts and assigns lower weights to abnormal observations, thereby weakening their influence on state estimation [33–35]. Its basic idea is to replace the standard least-squares criterion with a weighted or penalty-type cost function so that the filtering update becomes less sensitive to large residuals. The measurement innovation is defined as follows:

$$\mathbf{r}_k = \mathbf{z}_k - \mathbf{H}_k\hat{\mathbf{x}}_{k|k-1}, \tag{15}$$

Under the robust framework, a weight matrix $\mathbf{w}_k$ is introduced, and the corrected measurement noise covariance can be expressed as follows:

$$\widetilde{\mathbf{R}}_k = \mathbf{W}_k^{-1}\mathbf{R}_k, \tag{16}$$

where the weight matrix $\mathbf{w}_k$ is usually adaptively determined from the residual magnitude or robust kernel functions, such as Huber or IGG functions, to suppress the influence of abnormal observations.

On this basis, the adaptive robust Kalman filter further introduces an online noise-statistics estimation mechanism to address time-varying noise characteristics. A common approach is to combine the Sage–Husa adaptive estimation concept and recursively update the measurement noise covariance [36–38]:

$$\mathbf{R}_k = (1-\beta)\mathbf{R}_{k-1} + \beta\left(\mathbf{r}_k\mathbf{r}_k^{\mathrm{T}} - \mathbf{H}_k\mathbf{P}_{k|k-1}\mathbf{H}_k^{\mathrm{T}}\right), \tag{17}$$

where $\beta \in (0,1)$ is the forgetting factor is used to balance historical information and current observations.

By combining robust weight correction and adaptive noise estimation, the filtering update equation of ARKF can be written as follows:

$$\begin{array}{c} \mathbf{K}_k = \mathbf{P}_{k|k-1}\mathbf{H}_k^{\mathrm{T}}\left(\mathbf{H}_k\mathbf{P}_{k|k-1}\mathbf{H}_k^{\mathrm{T}} + \widetilde{\mathbf{R}}_k\right)^{-1} \\ \hat{\mathbf{x}}_{k|k} = \hat{\mathbf{x}}_{k|k-1} + \mathbf{K}_k\mathbf{r}_k \\ \mathbf{P}_{k|k} = (\mathbf{I} - \mathbf{K}_k\mathbf{H}_k)\mathbf{P}_{k|k-1} \end{array}, \tag{18}$$

In this experiment, to address the non-Gaussian and time-varying characteristics of common observation noise in structural deformation monitoring in complex engineering environments. The filter state vector is defined as:

$$\mathbf{x}_k = \begin{bmatrix} p_k \\ v_k \end{bmatrix}, \tag{19}$$

where p_k and v_k denote the displacement and velocity states at epoch k, respectively. Assuming a constant-velocity motion model, the state-transition equation is expressed as:

$$\mathbf{x}_{k|k-1} = \mathbf{A}\mathbf{x}_{k-1|k-1} + \mathbf{w}_k, \tag{20}$$

where the state-transition matrix is:

$$\mathbf{A} = \begin{bmatrix} 1 & \Delta t \\ 0 & 1 \end{bmatrix}, \tag{21}$$

$$\mathbf{w}_k \sim N(0, \mathbf{Q}), \tag{22}$$

where Δt denotes the sampling interval, and $\mathbf{w}_k$ represents the process noise, which is assumed to follow a zero-mean Gaussian distribution with covariance matrix $\mathbf{Q}$. The observation model is formulated as:

$$z_k = \mathbf{H}\mathbf{x}_k + v_k, \tag{23}$$

where the observation matrix is $\mathbf{H} = \begin{bmatrix} 1 & 0 \end{bmatrix}$, $v_k \sim N(0, R)$.

z_k denotes the displacement observation and v_k represents the measurement noise with covariance matrix R.

To improve robustness against abnormal observations and time-varying disturbances, a residual-based adaptive weighting strategy is incorporated into the filtering process. The innovation residual is calculated as:

$$r_k = z_k - Hx_{k|k-1}, \tag{24}$$

Based on the innovation residual, the normalized innovation statistic is defined as:

$$d_k = \frac{r_k^2}{HP_{k|k-1}H^T + R}, \tag{25}$$

where $P_{k|k-1}$ denotes the predicted error covariance matrix and R_0 represents the nominal measurement noise variance. A threshold-based robust weighting mechanism is adopted to identify abnormal observations.

When $d_k \leq 3$, the observation is regarded as normal and the measurement noise covariance remains unchanged $R_k = R_0$.

When $d_k > 3$, the observation is considered to contain abnormal disturbances, and the measurement noise covariance is adaptively adjusted according to $R_k = R_0\left(\frac{d_k}{3}\right)$.

In this study, the process noise covariance matrix was set as Q = diag(1×10^{-5}, 1×10^{-7}), the nominal measurement noise variance was initialized as $R_0 = 5 \times 10^{-5}$, and the initial state covariance matrix was defined as P_0 = diag(1×10^{-4}, 1×10^{-6}). A robust threshold of d = 3 was adopted to identify abnormal observations and perform adaptive covariance inflation.

By integrating robustness and adaptivity, ARKF can effectively suppress the influence of abnormal observations and noise mismatch on filtering results without requiring accurate prior noise statistics, thereby substantially improving the stability and estimation accuracy of multi-source information fusion in complex environments. This property gives ARKF strong engineering applicability in GNSS/ACC fusion, structural health monitoring, and engineering navigation.

2.4. Construction of the WOA-VMD-ARKF Deformation Monitoring Algorithm

Considering the significant differences between GNSS and accelerometer signals in spectral structure and error mechanisms, this study adopts differentiated VMD modal reconstruction strategies to preprocess the two types of observations.

For GNSS position or velocity sequences, the effective motion information is mainly distributed in the low- and medium–low-frequency bands, whereas multipath effects, signal blockage, and random disturbances usually appear as high-frequency or abrupt components. Therefore, after VMD of GNSS signals, the low- and medium-frequency modes are retained while high-frequency noise modes are removed, thereby smoothing and denoising the observation sequence and improving the temporal consistency and reliability of GNSS observations. For accelerometer signals, low-frequency components are generally closely related to bias drift and slowly varying systematic errors, high-frequency components are dominated by random noise, and medium-frequency components mainly reflect the true motion characteristics of the carrier. Thus, based on VMD, this study removes the lowest- and highest-frequency modes and retains only the intermediate modes for signal reconstruction. This effectively suppresses bias accumulation and high-frequency noise interference and provides stable input for subsequent integration and state estimation [39].

At the state-estimation stage, an Adaptive Robust Kalman Filter (ARKF) is employed to address the non-Gaussian and non-stationary characteristics of observation noise frequently encountered in structural deformation monitoring. The filter incorporates a residual-based robust weighting mechanism to suppress the influence of abnormal observations and outliers, together with an adaptive covariance adjustment strategy that continuously updates noise statistics to accommodate time-varying measurement uncertainties. As a result, the proposed WOA–VMD–ARKF framework forms a hierarchical optimization architecture spanning both the signal-processing and state-estimation domains. The WOA–VMD module performs adaptive signal enhancement through optimal parameter selection and signal reconstruction, thereby improving the quality of GNSS and accelerom-

eter observations, whereas the ARKF ensures robust and reliable multi-sensor fusion under uncertain noise conditions. Through the coordinated optimization of observation quality and state estimation, the proposed framework achieves enhanced deformation-tracking performance and improved consistency among heterogeneous monitoring data. The parameter configurations and workflow of the proposed WOA–VMD–ARKF framework are presented in the following sections (Figure 2 and Table 1).

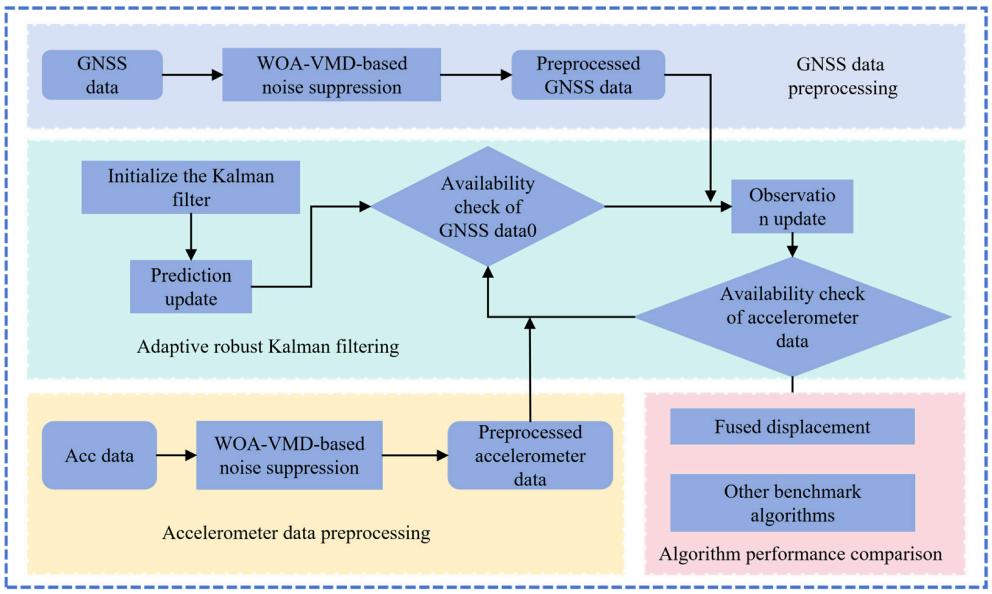


Figure 2. Technical route of the proposed method.

Table 1. Main parameters of the proposed WOA-VMD-ARKF framework.

Module	Parameter	Value
WOA	Population size	30
	Maximum iteration	50
VMD	K range	[2, 10]
	α range	[450–5600]
ARKF	Q	$\mathrm{diag}(1 \times 10^{-6}, 1 \times 10^{-8})$
	R_0	5.4×10^{-5}
	Threshold	3

The robustness of the proposed WOA-VMD-ARKF under non-Gaussian disturbances is evaluated through both numerical simulations and field experiments. The results demonstrate that the adaptive covariance adjustment strategy and residual-based robust weighting mechanism effectively mitigate the influence of observation outliers, multipath effects, and time-varying measurement noise, thereby improving the robustness and reliability of deformation estimation under complex monitoring conditions. Although the proposed method exhibits satisfactory performance in the investigated scenarios, several aspects warrant further investigation. First, the theoretical stability and convergence properties of the filter under strongly non-Gaussian stochastic processes have not yet been rigorously established. Second, the sensitivity of the framework to different initialization conditions, decomposition boundaries, and optimization parameter settings has not been systematically evaluated. Furthermore, repeatability analyses based on multiple independent monitoring datasets and diverse environmental conditions remain to be conducted. Future studies will focus on integrating additional practical engineering monitoring scenarios, conducting comprehensive sensitivity and repeatability assessments, and performing systematic theoretical analyses of filter stability and convergence. These efforts are expected

to further strengthen the theoretical foundation of the proposed framework and facilitate its broader application in structural deformation monitoring and engineering practice.

3. Numerical Simulation Experiments

3.1. Simulation Signal Generation

To systematically verify the applicability and robustness of the proposed WOA-VMD-ARKF algorithm in super high-rise building deformation monitoring, a multi-frequency composite cosine signal simulation scheme is designed by considering the low-frequency quasi-static deformation and high-frequency micro-vibration characteristics of super high-rise buildings, together with the complementary sensing characteristics of GNSS and accelerometers, as follows:

$$x(t) = A_1 \sin(2\pi f_1 t) + A_2 \sin(2\pi f_2 t + \phi_1) + A_3 \sin(2\pi f_3 t + \phi_2), \tag{26}$$

where

$A_1 = 0.002$ m, $A_2 = 0.0012$ m, and $A_3 = 0.0008$ m are the amplitudes of the displacement signal, representing the vibration amplitudes of different frequency components;

$f_1 = 0.15$ Hz, $f_2 = 0.35$ Hz, and $f_3 = 0.75$ Hz are the dominant frequency components of the displacement signal, covering responses from low-frequency quasi-static deformation to medium- and high-frequency dynamics;

$\phi_1 = \pi/4$ and $\phi_2 = \pi/6$, the phase terms of each high-frequency component are adopted to simulate asynchronous vibration characteristics.

The corresponding true acceleration is derived directly from the second derivative of the displacement signal, ensuring physical consistency between displacement and acceleration. Its expression is:

$$\begin{aligned} a(t) = \ddot{x}(t) = &-A_1(2\pi f_1)^2 \sin(2\pi f_1 t) \\ &-A_2(2\pi f_2)^2 \sin(2\pi f_2 t + \phi_1) \\ &-A_3(2\pi f_3)^2 \sin(2\pi f_3 t + \phi_2) \end{aligned}, \tag{27}$$

The GNSS signal is sampled at 1 Hz and mainly captures low-frequency quasi-static displacement components. To simulate realistic GNSS observation errors, Gaussian white noise and low-frequency slowly varying drift are added. The acceleration signal is sampled at 100 Hz to capture high-frequency dynamic deformation components. To simulate realistic accelerometer measurement errors, Gaussian white noise and high-frequency vibration noise are superimposed. This model not only ensures the physical consistency of displacement and acceleration but also simulates typical error characteristics of GNSS/accelerometer observations in practical applications, providing reliable simulation data for subsequent validation of denoising algorithms and fusion positioning methods (Figures 3 and 4).

To verify the denoising performance of the GNSS/ACC fusion positioning algorithm, this study constructs a numerical simulation dataset containing both GNSS multipath errors and accelerometer high-frequency noise. The GNSS displacement sequence is generated using a mixed cosine signal superimposed with multi-frequency sinusoidal components, effectively reproducing the quasi-periodic fluctuation characteristics of multipath interference. The acceleration sequence is superimposed with broadband white noise typical of inertial sensors. This provides a physically meaningful benchmark scenario for subsequent comparison of the denoising effects of EMD, VMD, and WOA-VMD.

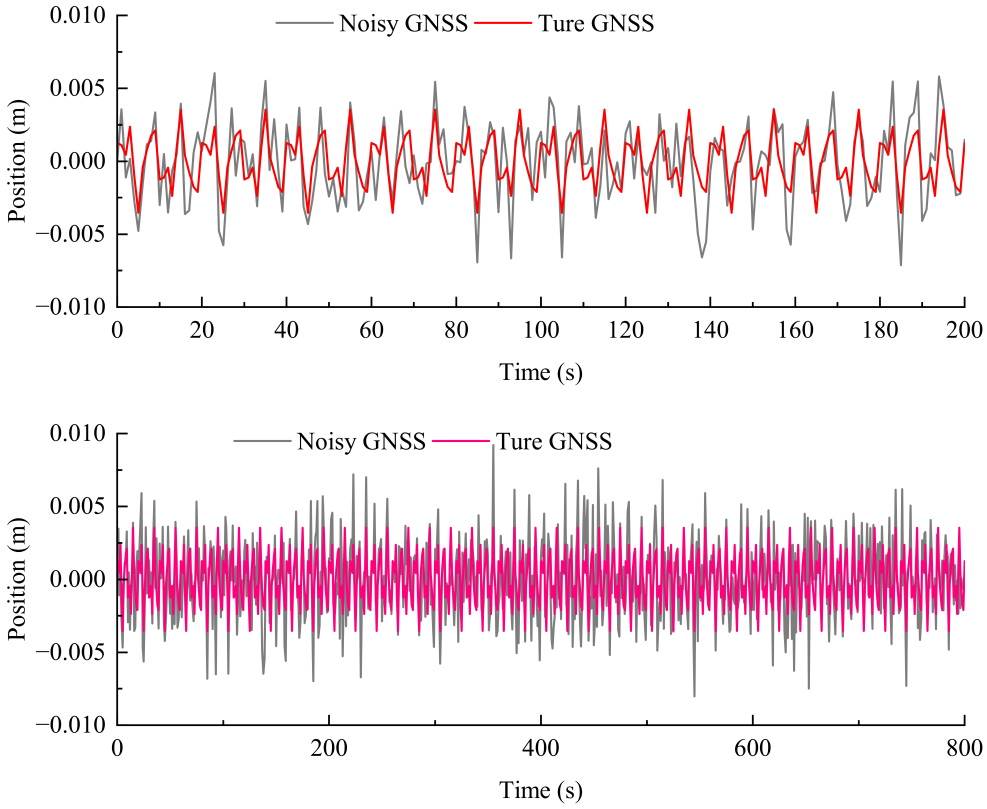


Figure 3. GNSS displacement over different time spans.

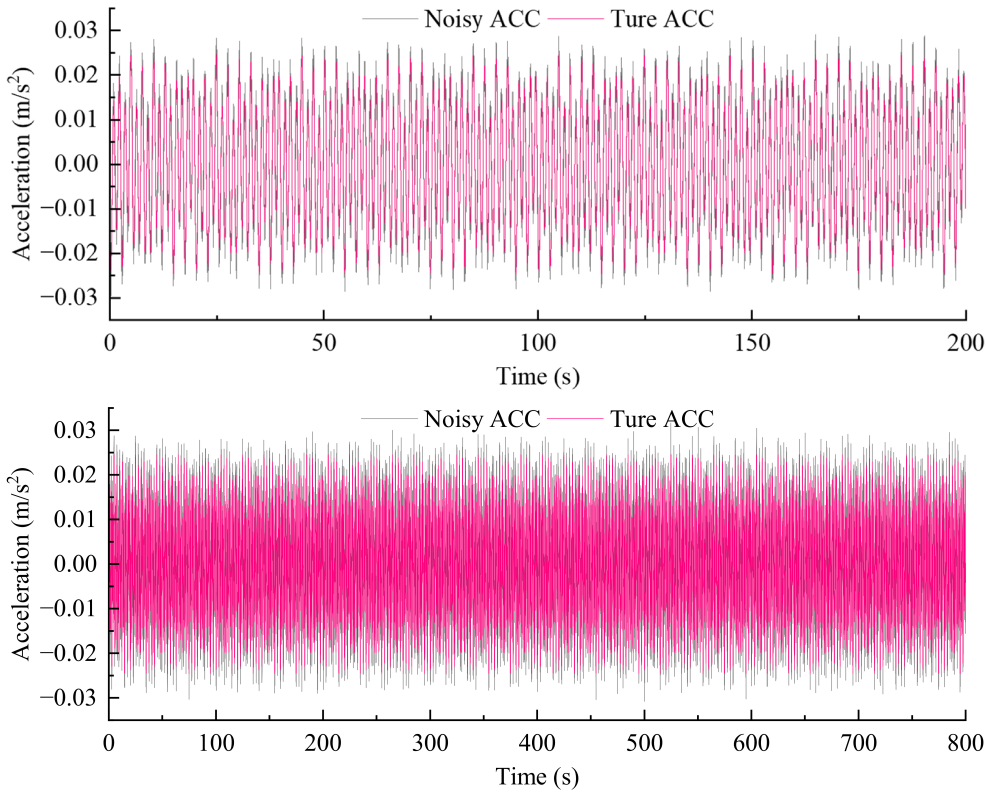


Figure 4. ACC variations over different time spans.

3.2. Analysis of Simulation Results

(1) Performance validation and comparative analysis of WOA-VMD for GNSS noise suppression

The comparative results for noise suppression in the GNSS displacement sequence are shown in Figure 5. The WOA-VMD algorithm demonstrates clear overall advantages in noise attenuation and signal-feature preservation. The processing results for short- and long-duration sequences show that the original noisy GNSS signal contains obvious quasi-periodic multipath fluctuations and random spike interference. Although EMD and VMD can partially suppress noise, significant residual fluctuations remain. In contrast, the sequence processed by WOA-VMD shows the highest consistency with the evolution trend of the true signal. For the short-duration data, the RMSE decreases to 0.085 cm and the SNR increases by 3.17 dB; for the long-duration data, the RMSE decreases to 0.115 cm and the SNR increases by 5.24 dB. The denoising effect is markedly better than those of EMD and VMD. These results confirm that WOA-VMD can adaptively optimize modal decomposition parameters using the whale optimization algorithm, thereby more effectively separating multipath error components from true displacement signals and providing high-fidelity preprocessed data for subsequent GNSS/ACC fusion positioning.

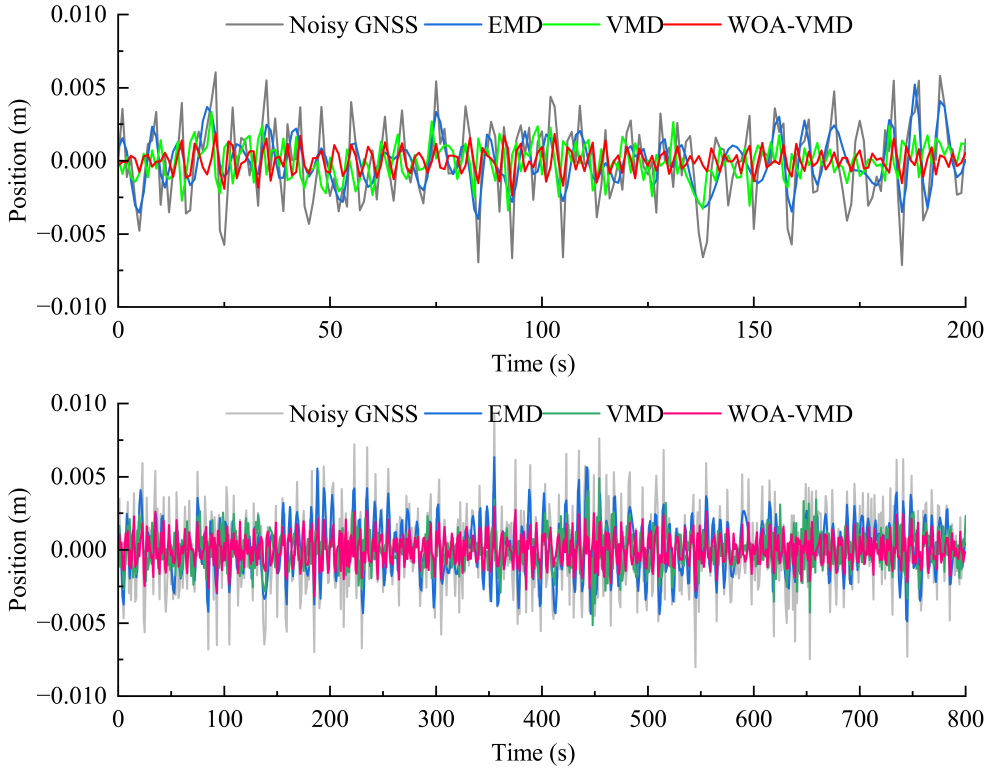


Figure 5. Comparison of denoising effects for GNSS displacement sequences.

(2) Performance comparison between VMD and WOA-VMD for accelerometer noise suppression

The comparative results for suppressing high-frequency accelerometer measurement noise are shown in Figure 6. The WOA-VMD algorithm has prominent advantages in noise filtering and signal preservation. It effectively suppresses high-frequency noise interference in the raw signal. For the short-duration data, the RMSE decreases to 0.87 cm and the SNR increases by 3.05 dB; for the long-duration data, the RMSE decreases to 0.132 cm and the SNR increases by 5.94 dB. Compared with EMD and standard VMD, WOA-VMD provides more stable denoising performance, avoids mode mixing and performance degradation under long-sequence operating conditions, and can provide high-SNR, high-fidelity inertial observation data for GNSS/ACC integrated positioning. These findings fully verify the effectiveness and reliability of the proposed method in high-frequency noise suppression scenarios.

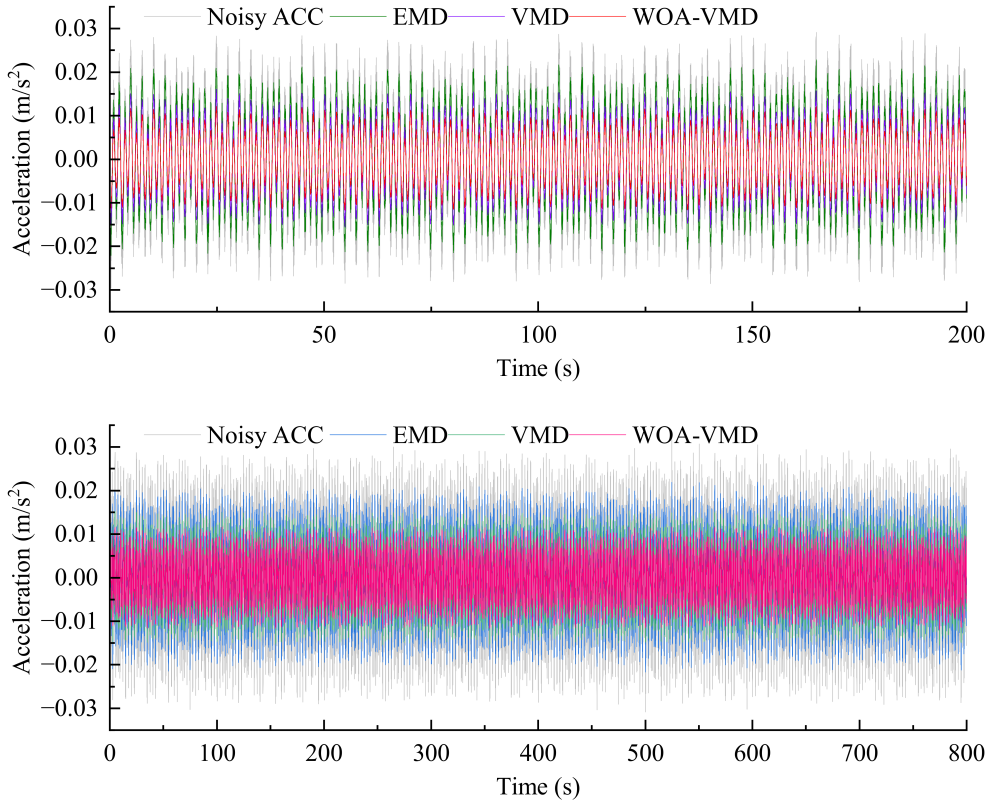


Figure 6. Comparison of denoising effects for ACC variation sequences.

(3) Effectiveness validation of the WOA-VMD-ARKF algorithm in GNSS/ACC data fusion

To verify the overall performance of the WOA-VMD-ARKF fusion positioning algorithm, it is compared with the conventional ARKF algorithm. The results show that the raw noisy signal is strongly affected by high-frequency interference and environmental disturbances, with displacement fluctuations reaching ±1 cm. Although the conventional ARKF can smooth the noise to some extent, obvious residual fluctuations remain. Under non-stationary noise conditions, its filtering performance tends to deteriorate, making it difficult to accurately recover the true displacement trend. In contrast, through hierarchical coordination between WOA-VMD signal preprocessing and adaptive robust Kalman filtering, the WOA-VMD-ARKF algorithm can simultaneously suppress GNSS low-frequency drift and high-frequency noise interference. The RMSEs for different time periods are reduced to 0.083 cm and 0.127 cm, and the SNRs increase by 3.94 dB and 6.10 dB, respectively, achieving an optimal balance between noise suppression and effective signal preservation. Overall, the proposed algorithm effectively compensates for the adaptability limitations of conventional ARKF in non-stationary noise environments and significantly improves positioning accuracy and temporal stability. Its performance gain essentially arises from the adaptive optimization of key VMD parameters by WOA, which enables accurate separation and efficient suppression of observation noise. These results provide highly reliable displacement monitoring data for structural health monitoring and fully demonstrate the effectiveness and superiority of the method in complex engineering scenarios. Because the simulation uses a multi-frequency cosine model for quantitative comparison, whereas actual structural responses are strongly random and non-stationary, this study further verifies the engineering applicability of the proposed method using field measurement data (Figure 7).

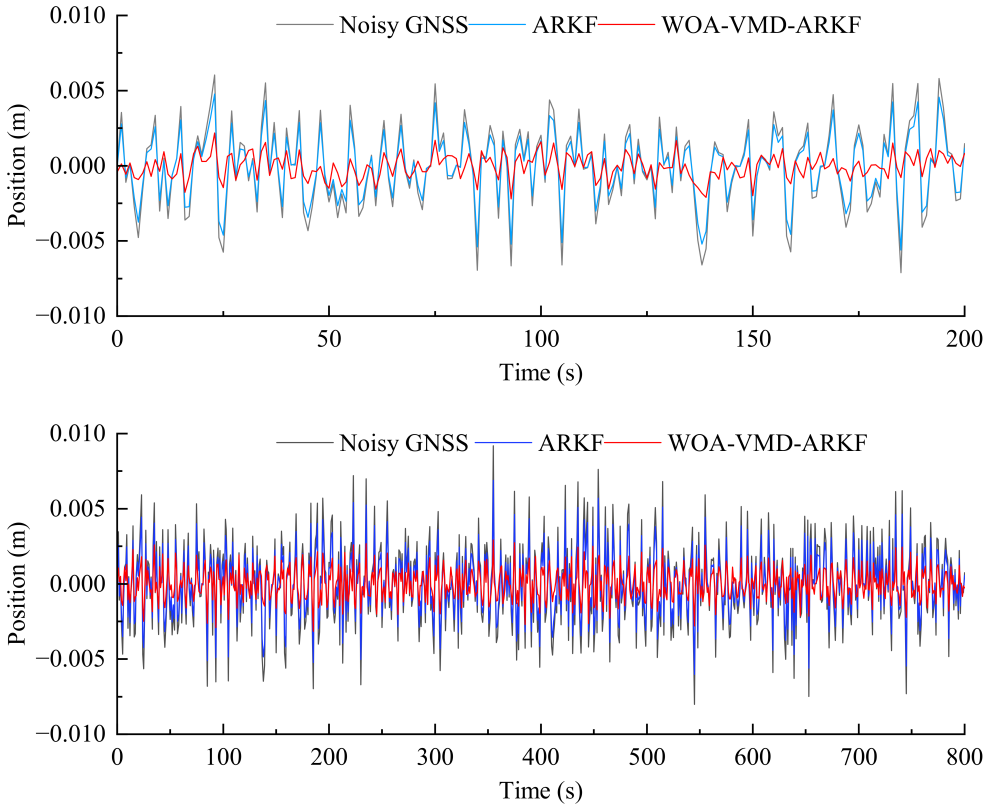


Figure 7. Comparison of denoising effects after fusion.

It should be noted that the numerical simulation adopted in this study is intended as a controlled benchmark for algorithm verification. Although the simulated signal incorporates multiple frequency components and measurement noise, it does not fully represent the stochastic and non-stationary characteristics of actual super high-rise building responses. Therefore, the effectiveness and practical applicability of the proposed framework are further evaluated using real monitoring data collected from a super high-rise building under construction.

4. Field Experimental Validation on a Super High-Rise Building

4.1. Experimental Object and Equipment Selection

In this study, a super high-rise building under construction is selected as the experimental object for structural dynamic deformation monitoring. The building adopts a combined load-bearing system consisting of a reinforced-concrete core tube and exterior frame columns. Its facade consists of a large-area glass curtain wall and vertical structural components. During construction, the structure is continuously subjected to coupled effects such as wind loads, construction disturbances, temperature gradients, and uneven foundation settlement. These effects can induce typical mechanical behaviors, including overall sway, inter-story relative displacement, and high-frequency vibration responses, making high-precision, long-duration, multi-source collaborative monitoring and feature analysis urgently needed [40,41]. In this study, an integrated BDS/GNSS and accelerometer sensing device is used for field data acquisition, and the overall monitoring equipment layout is shown in Figure 8. The reference station is installed on the open top of a nearby structure with stable geological conditions and unobstructed satellite signals, while the monitoring station is installed at key load-bearing and deformation-sensitive positions of the super high-rise building. This arrangement enables long-term continuous and synchronized observation of structural static displacement and dynamic vibration informa-

tion. The deployment strictly follows construction-period monitoring safety specifications, does not interfere with the main construction procedures, and satisfies the requirements of unobstructed observation, low multipath, and easy maintenance, thereby providing high-quality and highly reliable raw observations for subsequent multi-source data fusion and deformation-feature estimation [42,43].



Figure 8. Schematic diagram of equipment installation.

The BDS receiver sampling frequency is set to 1 Hz, while the accelerometer collects data synchronously at a high frequency of 100 Hz. The two sensors respectively acquire low-frequency static time series and high-frequency vibration time series of the building. The specifications of the BDS receiver and accelerometer used in this study are listed in Table 2.

Table 2. Main specifications of the GNSS receiver and accelerometer.

Method		Value
GNSS	Signal tracking	BDS: B1/B2/B3; GPS: L1/L2/L5; GALILEO: E1/E5a/E5b; QZSS: L1/L5
	RTK (RMS)	Horizontal: ±8 mm + 1 ppm; Vertical: ±15 mm + 1 ppm
	Update rate	1 Hz
ACC	Range	±2 g/±4 g/±8 g
	Resolution	0.01 mg
	Accuracy	0.1 mg

For consistency, GNSS observations are expressed in the local East–North–Up (ENU) coordinate system, whereas accelerometer measurements are recorded in the sensor-fixed X–Y–Z coordinate system. During sensor installation, the accelerometer axes were aligned with the ENU directions; therefore, the X-, Y-, and Z-axes correspond to the East (E), North (N), and Up (U) directions, respectively. Unless otherwise stated, E/X, N/Y, and U/Z denote the same physical directions throughout this study.

4.2. Accuracy Validation of Fusion Results

To ensure the geometric consistency and physical comparability of GNSS and accelerometer data fusion, axis alignment and attitude calibration are strictly performed during sensor installation. The sensitive axes of the accelerometer are precisely aligned with the structural coordinate system of the building, namely the east (E), north (N), and vertical (U) directions, using mechanical fixtures. Initial orientation calibration is then completed using attitude sensors, such as a high-precision inclinometer or electronic compass, to ensure that the observation dimensions of the two sensor types are strictly mapped to the same three-dimensional deformation reference. This eliminates the influence of axis misalignment on fusion accuracy at the hardware level and provides geometric constraints for spatiotemporal synchronization and fusion of multi-source data.

The experiment uses three hours of continuous monitoring data collected on 12 September 2025. The data cover a scenario in which static micro-deformation of the super high-rise building is coupled with environmental vibration, and include typical error components such as multipath interference, high-frequency vibration noise, and low-frequency drift. They can therefore comprehensively verify the accuracy stability and noise robustness of the fusion algorithm under complex operating conditions. It should be noted that, because no high-precision external ground-truth reference is available in the field experiment, the denoised GNSS results are used as a relative evaluation benchmark to compare the performance differences among different methods, rather than to assess absolute accuracy.

Using the raw GNSS displacement sequence as the comparison baseline, the fusion-result accuracy is systematically evaluated in the three-dimensional directions (E/N/U) using three core quantitative indicators: root mean square error (RMSE), signal-to-noise ratio (SNR), and standard deviation (STD), together with time-domain waveform characteristics. The statistical results are shown in Table 3.

Table 3. GNSS denoising accuracy evaluation.

Method	Metric	Denoised Result	Raw GNSS	Improvement
E	RMSE/cm	1.03	2.15	51.9%
	SNR/dB	19.37	15.19	4.18
	STD/cm	0.79	1.86	57.5%
	PSD (dB)	5.82	−2.06	7.88
N	RMSE/cm	0.91	2.33	60.9%
	SNR/dB	18.54	14.08	4.46
	STD/cm	0.81	2.01	59.7%
	PSD (dB)	6.15	−2.14	8.19
U	RMSE/cm	1.92	3.57	46.3%
	SNR/dB	14.64	10.76	3.88
	STD/cm	1.51	3.29	54.1%
	PSD (dB)	4.06	−3.38	7.44

Figure 9 presents three-dimensional raw GNSS displacement time series for the east (E), north (N) and up (U) components, as well as denoising comparison results from the Kalman filter (KF), conventional variational mode decomposition (VMD), empirical mode decomposition (EMD), complete ensemble empirical mode decomposition with adaptive noise (CEEMDAN), and the proposed WOA-VMD algorithm. Affected by multipath effects, coupled environmental vibrations and stochastic noise, the raw GNSS displacement sequences feature conspicuous high-frequency burrs and local anomalous spikes in all three dimensions. The noise fluctuations are particularly drastic in the vertical direction, with displacement deviations reaching ±4 cm, making the raw data inappropriate for

direct extraction of structural deformation characteristics. The KF merely smooths data based on temporal statistical properties and struggles to suppress large-amplitude impulse noise, such that remarkable anomalous fluctuations remain in the processed time series. Standard VMD separates noise by predefining the number of decomposition modes; nevertheless, its parameters require manual empirical configuration and suffer insufficient adaptability to varying noise levels. Residual obvious high-frequency noise components persist after VMD processing under strong vertical interferences. Although EMD smooths noise to a certain extent, it is plagued by mode mixing, offers limited suppression of sharp spikes, and tends to generate spurious fluctuations. CEEMDAN effectively alleviates the mode mixing issue of EMD by introducing auxiliary noise, yet its performance in removing intense impulse interferences remains unsatisfactory. By contrast, the WOA-VMD algorithm implements adaptive optimization of critical VMD parameters through the whale optimization algorithm, enabling accurate separation of valid signals and noise components. The waveform smoothness of the denoised three-dimensional sequences is greatly enhanced; anomalous spikes are effectively restrained, and the low-frequency deformation trends of structural displacements are fully retained without evident phase distortion or amplitude bias. As summarized in Table 3, after denoising, the horizontal RMSEs drop to 1.03 cm and 0.91 cm, corresponding to reductions of 51.9% and 60.9% compared with raw data; the PSDs improve to 5.82 dB and 6.15 dB; the SNRs rise to 19.37 dB and 18.54 dB, indicating a substantial increase in the proportion of valid signals; and the STDs are reduced to 0.79 cm and 0.81 cm, which reflects markedly improved data stability. The vertical component is most severely disturbed by multipath effects. Following WOA-VMD denoising, the vertical RMSE decreases to 1.92 cm (a 46.3% reduction from raw measurements), the SNR increases to 14.64 dB, and the STD falls to 1.51 cm. The proposed method effectively addresses the bottleneck of insufficient vertical observation precision for GNSS and delivers high-quality GNSS displacement observations to facilitate subsequent integrated positioning combining GNSS and accelerometer data.

Similarly, targeted denoising analysis is performed on the synchronously collected ACC data. This is intended to address the problem that, in super high-rise building monitoring, ACC data are easily affected by environmental vibration, sensor thermal noise, and electromagnetic interference, resulting in high-frequency clutter, baseline drift, and local abnormal disturbances. The analysis ensures the validity and accuracy of the ACC data and provides high-quality acceleration data for GNSS/ACC fusion. The time-domain waveform comparison is shown in Figure 10.

The denoising effect is systematically verified using the three core indicators RMSE, SNR, and STD, together with time-domain waveform characteristics, and is compared with the raw ACC data. The statistical results are shown in Table 4.

Figure 10 displays the raw triaxial acceleration time series (X, Y, Z) acquired by the accelerometer, together with processed curves obtained using various denoising approaches, including KF, VMD, EMD, CEEMDAN and the proposed WOA-VMD algorithm. Contaminated by sensor thermal noise, coupled environmental vibrations and high-frequency clutter, the raw triaxial acceleration signals are characterized by prominent random fluctuations and local sharp spikes. The valid signal components are severely submerged by noise; direct integration of such noisy signals for displacement calculation readily introduces drift errors, which substantially deteriorate the accuracy and reliability of subsequent deformation inversion via multi-source data fusion. Conventional denoising algorithms possess inherent drawbacks when handling non-stationary acceleration signals. The KF can only mitigate mild stochastic noise and exhibits weak capacity to suppress abrupt impulse interferences, leaving abundant anomalous components in the post-processed triaxial acceleration sequences. In contrast to EMD, which is susceptible to mode mix-

ing, and standard VMD, whose parameters rely on manual empirical tuning, CEEMDAN improves the stability of signal decomposition yet still fails to thoroughly eliminate intense impulse noise. The WOA-VMD algorithm proposed in this study achieves effective suppression of non-stationary noise and precise preservation of structural vibration signatures via adaptive parameter optimization, supplying high-fidelity observations for subsequent displacement reconstruction. Table 4 further verifies the superiority of the WOA-VMD algorithm. After denoising, the RMSEs of the three axes decline to 1.85 cm/s^2, 2.07 cm/s^2 and 2.41 cm/s^2, representing reductions ranging from 49.7–51.4% relative to the raw data. The PSDs increase to 5.56 dB, 5.32 dB and 3.24 dB; the SNRs rise to 19.02 dB, 18.86 dB and 17.16 dB, while the STDs decrease to the range of 1.71–2.17 cm/s^2. Overall, the noise suppression performance of WOA-VMD along all three axes significantly outperforms KF, VMD, EMD and CEEMDAN. The proposed algorithm demonstrates stronger robustness under severe high-frequency noise conditions and can provide high-quality inertial observation data to support subsequent integrated positioning combining GNSS and accelerometer (ACC) measurements.

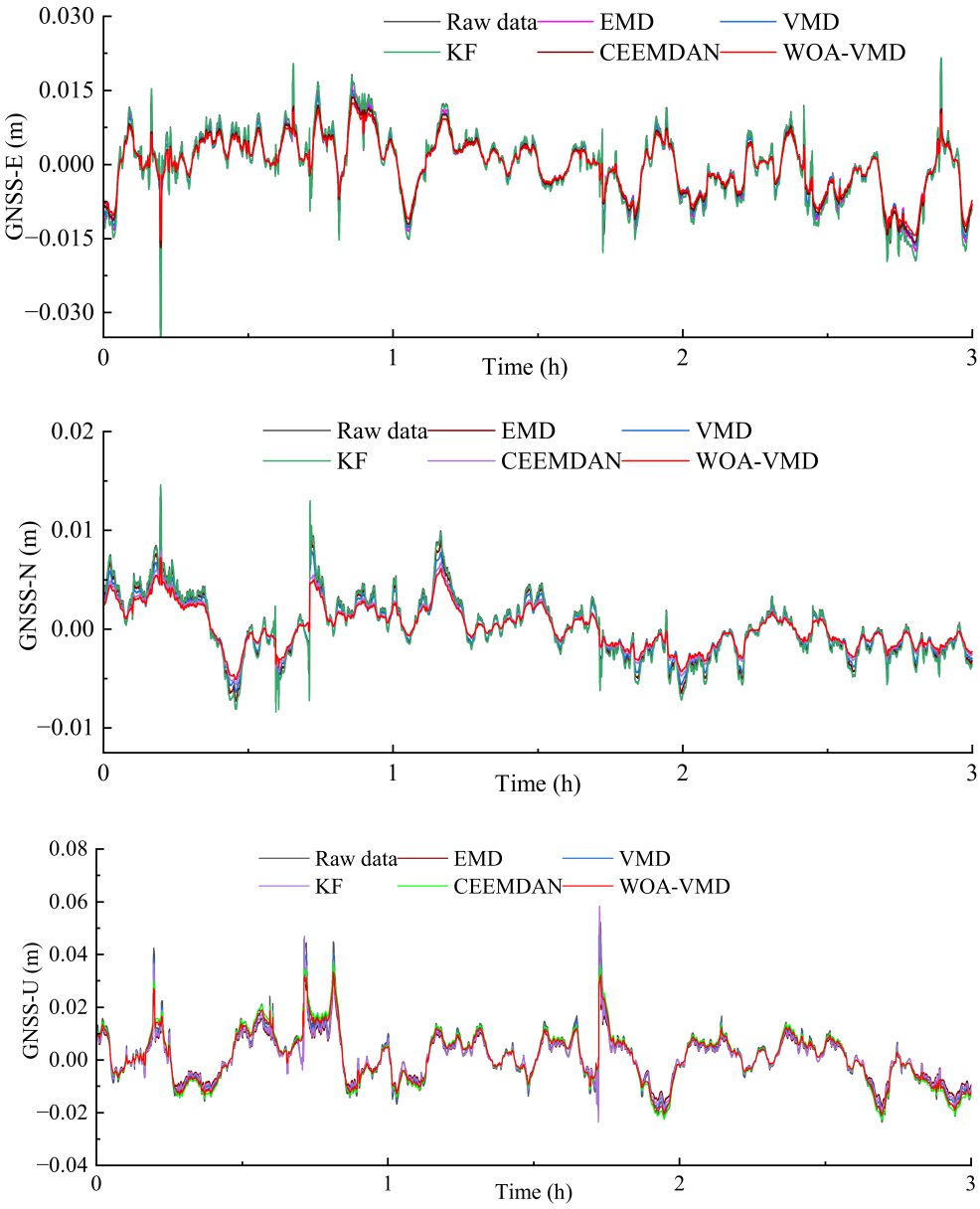


Figure 9. Comparison of denoising effects for three-dimensional GNSS displacement sequences.

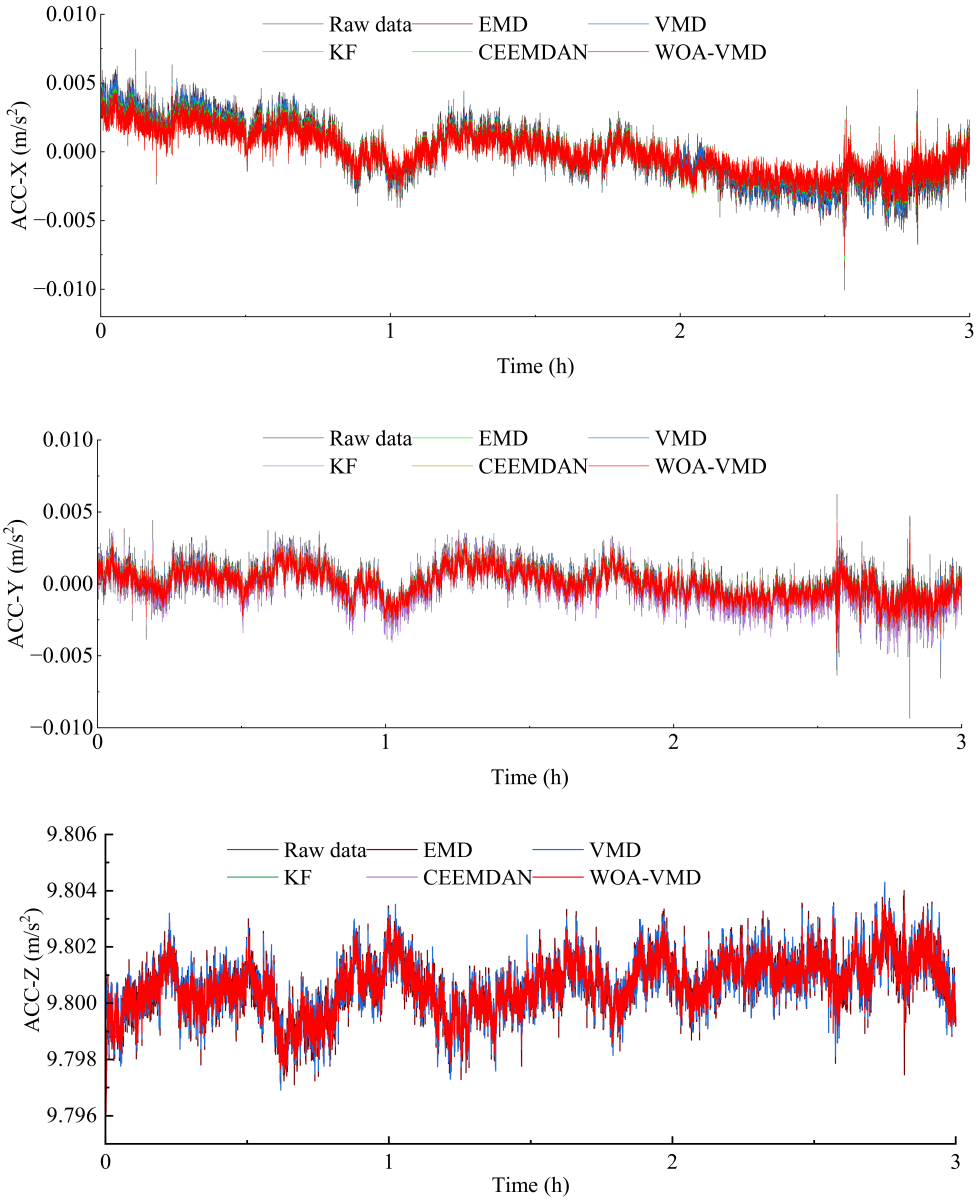


Figure 10. Comparison of denoising effects for three-dimensional ACC data.

Table 4. Accuracy evaluation of ACC denoising.

Method	Metric	Denoised Result	Raw ACC	Improvement
X	RMSE/cm/s^2	1.85	3.81	51.4%
	SNR/dB	19.02	14.28	4.74
	STD/cm/s^2	1.71	3.54	51.6%
	PSD (dB)	5.56	−2.35	7.91
Y	RMSE/cm/s^2	2.07	4.16	50.3%
	SNR/dB	18.86	13.76	5.10
	STD/cm/s^2	1.83	3.71	50.6%
	PSD (dB)	5.32	−2.77	8.09
Z	RMSE/cm/s^2	2.41	4.79	49.7%
	SNR/dB	17.16	12.93	4.23
	STD/cm/s^2	2.17	4.38	50.4%
	PSD (dB)	3.24	−4.02	7.26

To verify the effectiveness and superiority of the WOA-VMD-ARKF fusion algorithm, multi-rate data fusion is implemented using a state-space model. GNSS updates observations at 1 Hz, while the accelerometer participates in state prediction at 100 Hz, thereby achieving spatiotemporal synchronization of multi-source observations. On this basis, an adaptive robust Kalman filtering framework is constructed to obtain the optimal fusion estimate of the two types of data. To systematically evaluate fusion performance, the fused displacement sequence is qualitatively and quantitatively compared with the GNSS displacement sequence denoised by WOA-VMD, as shown in Figure 11.

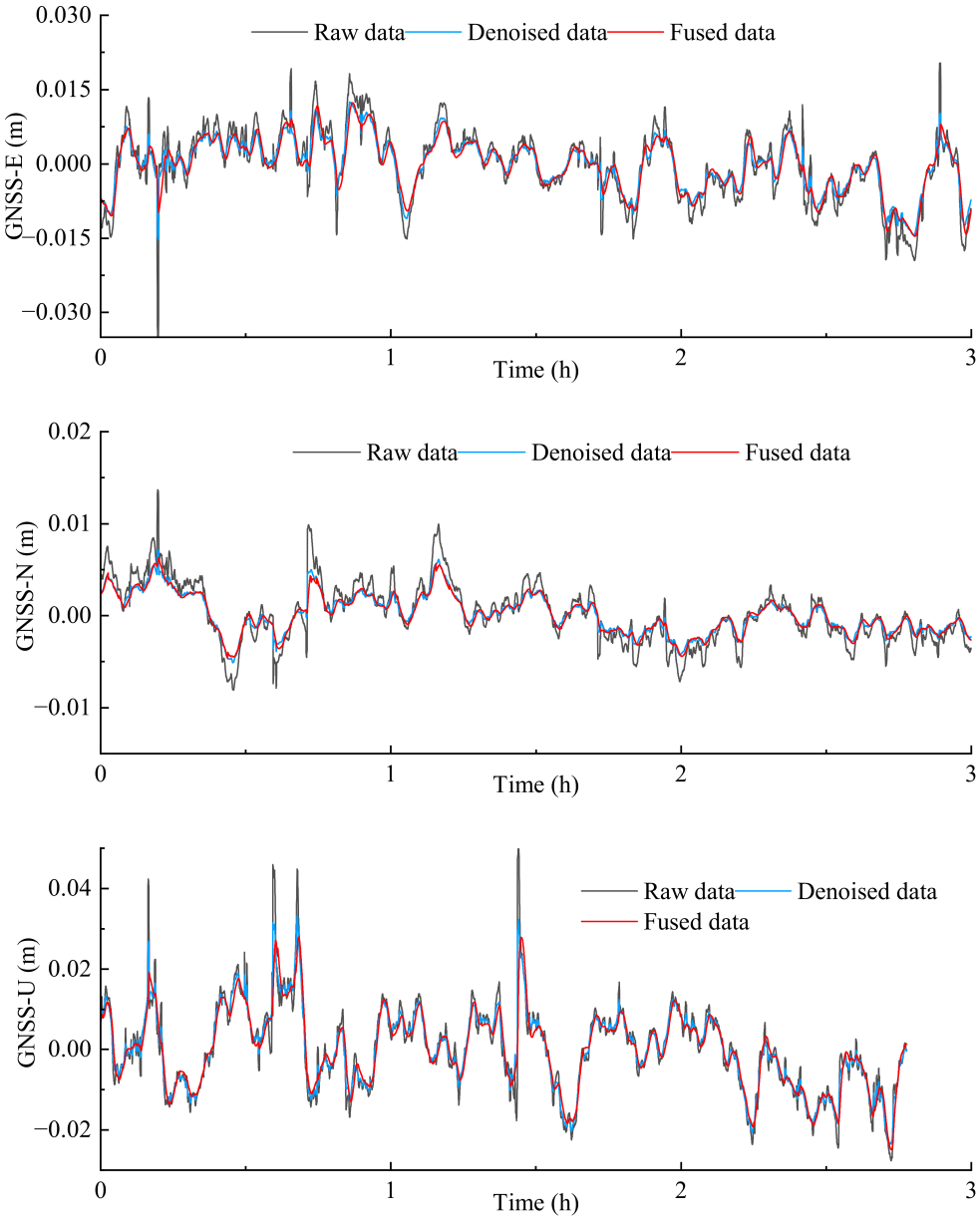


Figure 11. Comparison of displacement sequences before and after GNSS/ACC fusion.

As shown in Figure 11, although the denoised GNSS displacement sequence has significantly suppressed multipath and high-frequency noise, small random fluctuations remain because of observation-system errors. After WOA-VMD-ARKF fusion, the smoothness of the displacement sequence is further improved, abnormal fluctuations are effectively suppressed, and the underlying low-frequency deformation trend of the structure is effectively preserved without evident phase distortion or amplitude offset. Table 5 lists the key accuracy indicators before and after fusion.

Table 5. Performance evaluation of GNSS/ACC fusion results.

Method	Metric	Raw GNSS	Denoised GNSS	Fused GNSS
E	RMSE/cm	2.15	1.03	0.67
	SNR/dB	15.19	19.37	22.03
	STD/cm	1.86	0.79	0.51
	PSD (dB)	−2.06	5.82	9.47
N	RMSE/cm	2.33	0.91	0.56
	SNR/dB	14.08	18.54	21.38
	STD/cm	2.01	0.74	0.49
	PSD (dB)	−2.14	6.15	9.02
U	RMSE/cm	3.57	1.92	1.42
	SNR/dB	10.76	14.64	16.74
	STD/cm	3.29	1.51	1.04
	PSD (dB)	−3.38	4.06	6.61

As shown in Table 5, multi-sensor fusion significantly improved the displacement monitoring performance in all three directions. In the horizontal directions, the RMSE values were reduced to 0.67 cm and 0.56 cm, respectively. Meanwhile, the corresponding SNR values increased to 22.03 dB and 21.38 dB, the PSD values increased to 9.45 dB and 9.02 dB, and the STD values decreased to 0.51 cm and 0.49 cm, respectively, indicating substantial improvements in signal quality, measurement stability, and deformation estimation consistency. The vertical component, which is inherently more susceptible to multipath interference, satellite geometry limitations, and environmental disturbances, also exhibited considerable improvement after fusion. Specifically, the RMSE decreased from 1.92 cm for the denoised GNSS observations to 1.42 cm after fusion, while the corresponding SNR, PSD, and STD values reached 16.74 dB, 6.61 dB, and 1.04 cm, respectively. These results demonstrate that the proposed framework effectively improves the monitoring performance of the vertical component and improves the consistency and reliability of displacement estimation.

It should be noted that no independent high-precision reference system, such as a total station or laser displacement sensor, was available during the field experiment. Consequently, the denoised GNSS observations were adopted as a relative benchmark for performance evaluation. Therefore, the reported results primarily demonstrate the noise-suppression capability and relative deformation-tracking performance of the proposed WOA–VMD–ARKF framework rather than its absolute measurement accuracy.

From an engineering perspective, the vertical component of GNSS-based deformation monitoring generally exhibits lower accuracy than the horizontal components due to unfavorable satellite geometry, stronger multipath effects, and higher sensitivity to environmental disturbances. Nevertheless, the achieved vertical monitoring performance remains meaningful for practical applications. According to the requirements specified in the 《Standard for Engineering Surveying》 and the《Code for Building Deformation Measurement》, the primary objective of structural deformation monitoring is to identify long-term deformation trends, abnormal structural responses, and cumulative displacements induced by foundation settlement, temperature variation, and construction activities. In practical super-tall building monitoring, the magnitude of vertical deformation is typically substantially greater than the monitoring uncertainty of 1.42 cm achieved in this study. Therefore, although the vertical monitoring performance remains lower than that of the horizontal directions, the significant reduction in vertical RMSE achieved through multi-source fusion demonstrates that the proposed framework can effectively capture structural deformation characteristics and provide practical support for routine engineering deformation monitoring [44,45].

From a structural engineering perspective, the monitored response characteristics are consistent with the expected behavior of a super-tall building under construction. The monitored structure has a design height of 339.9 m, and its deformation response is influenced by multiple factors, including progressive gravity loading from ongoing construction activities, temporary construction loads, wind excitation, and environmental effects. Consequently, the structural response contains both low-frequency quasi-static deformation components and high-frequency dynamic vibration components.

The GNSS observations primarily capture long-term deformation trends, including gradual settlement and lateral displacement induced by construction loading and environmental actions. In contrast, the accelerometer measurements are more sensitive to high-frequency structural vibrations caused by wind excitation, equipment operation, and construction activities. Therefore, neither sensor alone can fully characterize the structural behavior of the monitored building. The proposed WOA–VMD–ARKF framework effectively integrates the complementary characteristics of GNSS and accelerometer observations. The fused displacement results preserve the low-frequency deformation trends while simultaneously capturing high-frequency dynamic responses. This behavior is consistent with the actual deformation mechanism of super-tall buildings during construction, where slow cumulative deformation and dynamic vibration coexist. The improved consistency between displacement and acceleration observations further demonstrates that the proposed framework can provide a more comprehensive representation of structural behavior than single-sensor monitoring approaches. Moreover, the achieved vertical monitoring performance is particularly valuable during the construction stage, as vertical deformation is directly related to cumulative settlement and construction-induced loading effects. Although the vertical component remains less accurate than the horizontal components due to inherent GNSS limitations, the significant reduction in monitoring uncertainty after fusion improves the capability to track vertical deformation evolution and assess structural behavior under ongoing construction conditions.

Overall, the proposed WOA–VMD–ARKF fusion framework effectively mitigates the effects of GNSS low-frequency drift and measurement noise through the integration of high-frequency accelerometer observations and adaptive Kalman-filtering-based error compensation. By exploiting the complementary characteristics of GNSS and accelerometer measurements, the framework significantly improves displacement monitoring performance while enhancing the consistency and reliability of multi-source observations in all three directions. The results demonstrate that the proposed framework provides an effective solution for structural deformation monitoring of super-tall buildings and exhibits improved noise-suppression and deformation-tracking capabilities compared with conventional GNSS-only approaches. Furthermore, the field validation confirms the feasibility and practical applicability of the proposed framework under complex monitoring environments characterized by multipath interference and non-stationary noise.

5. Conclusions

To meet the demand for high-precision dynamic micro-deformation monitoring of super high-rise buildings during service, this study proposes a GNSS/accelerometer fusion monitoring method based on whale optimization algorithm–optimized variational mode decomposition (WOA-VMD) and adaptive robust Kalman filtering (ARKF). The method is used for high-precision sensing of dynamic micro-deformation in super high-rise buildings. The field results indicate the following:

(1) The WOA-VMD method significantly enhances signal denoising performance while preserving deformation-related characteristics. Compared with EMD and conventional VMD, the proposed approach adaptively optimizes the number of decompo-

sition modes and penalty factors using WOA, effectively suppressing mode mixing and improving the separation of deformation signals from noise components. For GNSS observations, the RMSE values in the east, north, and vertical directions were reduced by 51.9%, 60.9%, and 46.3%, respectively; the corresponding STD values were reduced by 57.5%, 59.7%, and 54.1%, while the SNR values increased by 4.18 dB, 4.46 dB, and 3.88 dB. For accelerometer measurements, the RMSE values of the three axes were reduced by 49.7%, 50.3%, and 51.4%, respectively; the STD values decreased by 50.4%, 50.6%, and 51.6%, while the SNR values increased by 4.23 dB, 4.74 dB, and 5.10 dB. These results demonstrate that the proposed method provides higher-quality observations for subsequent data fusion.

(2) The proposed WOA-VMD-ARKF framework substantially improves displacement monitoring performance. After fusion, the RMSE and STD of the displacement estimates were reduced by up to 75.97% and 75.62%, respectively, while the SNR increased to a maximum of 22.03 dB. The framework exhibited sub-centimeter-level displacement monitoring performance in the horizontal directions (E: 0.67 cm; N: 0.56 cm) and markedly enhanced the monitoring capability of the vertical component (U: 1.42 cm). Compared with standalone GNSS observations and conventional filtering approaches, the proposed framework demonstrated superior noise suppression and deformation-tracking capability.

(3) The WOA-VMD-ARKF framework exhibits strong robustness and practical applicability for structural deformation monitoring. Under complex urban environments characterized by multipath interference, non-stationary noise, and observation outliers, the proposed framework effectively suppresses noise and systematic disturbances while preserving both low-frequency settlement trends and high-frequency vibration characteristics. By integrating the long-term stability of GNSS observations with the high dynamic sensitivity of accelerometers, the framework provides an effective solution for structural deformation monitoring and dynamic response identification of super high-rise buildings. The results further demonstrate its potential for future structural health monitoring and safety assessment applications. Moreover, the proposed framework shows considerable promise for promoting more adaptive, reliable, and real-time deformation monitoring of large-scale civil infrastructures.

It should be noted that several limitations remain in the present study. First, the field-monitoring dataset is relatively limited in duration and does not cover extreme wind events, seasonal environmental variations, construction-stage disturbances, or long-term operational conditions. Second, the proposed fusion framework does not explicitly consider sensor installation errors, attitude-coupling effects, or structural model uncertainties, which may influence monitoring performance under complex engineering scenarios. Consequently, the current field validation primarily demonstrates the short-term feasibility and effectiveness of the proposed framework rather than its comprehensive applicability to long-term structural health monitoring. Future research will focus on validating the proposed framework using long-term monitoring datasets acquired under diverse environmental and loading conditions to further assess its stability, robustness, and generalization capability. In addition, structural dynamic models and multi-sensor collaborative observation mechanisms will be incorporated to strengthen the physical interpretability and adaptability of the fusion process. Furthermore, advanced machine-learning and data-driven approaches, including HCVCM, SVCM, and other emerging intelligent modeling techniques, will be explored and systematically compared with the proposed framework. Such investigations are expected to further enhance deformation-monitoring performance, improve robustness under complex noise environments, and promote the development of more reliable and intelligent monitoring systems for super high-rise structures.

Author Contributions: Conceptualization, J.W.; Investigation, L.Y.; Methodology, L.Y. and J.W.; Validation, L.Y., J.W., Y.J., P.W., P.Z. and Y.Y.; Writing—original draft, L.Y.; Writing—review & editing, L.Y. and J.W. All authors have read and agreed to the published version of the manuscript.

Funding: This work was supported by the National Natural Science Foundation of China (42274029).

Data Availability Statement: The data presented in this study are available in the article.

Conflicts of Interest: Author Yulong Jiang and Yilong Yu were employed by the company China State Construction Hongda Engineering Co., Ltd. The remaining authors declare that the research was conducted in the absence of any commercial or financial relationships that could be construed as a potential conflict of interest.

References

1. Ilgın, H.E.; Aslantamer, Ö.N. Investigating space utilization in skyscrapers designed with prismatic form. *Buildings* **2024**, *14*, 1295. [CrossRef]
2. Zhang, X.; Zhang, Y.; Li, B.; Qiu, G. GNSS-based verticality monitoring of super-tall buildings. *Appl. Sci.* **2018**, *8*, 991.
3. Wang, S.; Yin, C.; Sun, Y.; Wang, J. Dynamic deformation analysis of super high-rise buildings by integrating GNSS and accelerometers. *Bull. Surv. Mapp.* **2024**, *8*, 66–72.
4. Wang, J.; Yu, Y.L.; Liu, G.; Liu, X.; Jiang, Y.; Han, H. Method and progress for GNSS multi-source fusion deformation monitoring in super-tall buildings. *Geomat. Inf. Sci. Wuhan Univ.* **2025**, *50*, 1065–1076.
5. Bao, Y.S.; An, Y.D.; Li, X.; Jiang, Y.; Wang, P. Dynamic monitoring data analysis of high-rise building climbing frame based on GNSS and accelerometer fusion. *Sci. Surv. Mapp.* **2025**, *50*, 20–27.
6. Huang, S.Q.; Duan, Z.Q.; Wu, J.R.; Chen, J.P. Monitoring of horizontal displacement of a super-tall structure during construction based on navigation satellite and robotic total station. *J. Tongji Univ. (Nat. Sci.)* **2022**, *50*, 138–146. [CrossRef]
7. Hayat, H.; Griffiths, T.; Brennan, D.; Lewis, R.P.; Barclay, M.; Weirman, C.; Philip, B.; Searle, J.R. The state-of-the-art of sensors and environmental monitoring technologies in buildings. *Sensors* **2019**, *19*, 3648. [CrossRef] [PubMed]
8. Shen, N.; Chen, L.; Liu, J.; Wang, L.; Tao, T.; Wu, D.; Chen, R. A review of global navigation satellite system (GNSS)-based dynamic monitoring technologies for structural health monitoring. *Remote Sens.* **2019**, *11*, 1001. [CrossRef]
9. Li, Q.; He, Y.; Zhou, K.; Han, X.; He, Y.; Shu, Z. Structural health monitoring for a 600 m high skyscraper. *Struct. Des. Tall Spec. Build.* **2018**, *27*, e1490. [CrossRef]
10. Xiong, C.; Shang, Z.; Wang, M. Improved hybrid denoising method for dynamic monitoring of a super-high-rise building based on a GNSS-RTK technique. *J. Struct. Eng.* **2024**, *150*, 04024116. [CrossRef]
11. Yang, Y.; Xu, W.; Gao, Z.; Yu, Z.; Zhang, Y. Research progress of SHM system for super high-rise buildings based on wireless sensor network and cloud platform. *Remote Sens.* **2023**, *15*, 1473. [CrossRef]
12. Chen, Y.Y.; Zheng, K.; Zhang, X.H.; Wu, M.K.; Wang, P.X.; Fu, W.J.; Liu, K.Z. GPS/Galileo/BDS overlapping frequencies multipath error analysis and modeling. *Acta Geod. Cartogr. Sin.* **2025**, *54*, 1427–1438.
13. El-Sheimy, N.; Youssef, A. Inertial sensors technologies for navigation applications: State of the art and future trends. *Satell. Navig.* **2020**, *1*, 2. [CrossRef]
14. Zheng, W.H.; Dan, D.H.; Cheng, W.; Xia, Y. Real-time dynamic displacement monitoring with double integration of acceleration based on recursive least squares method. *Measurement* **2019**, *141*, 460–471. [CrossRef]
15. Shishegaran, A.; Varaee, H.; Rabczuk, T.; Shishegaran, G. High correlated variables creator machine: Prediction of the compressive strength of concrete. *Comput. Struct.* **2021**, *247*, 106479. [CrossRef]
16. Shishegaran, A.; Samadi, M.; Torabi, M. Novel Computational Methods to Predict the Compressive Strength of Hydrothermally Solidified Clay. *Front. Struct. Civ. Eng.* **2025**, *19*, 2054–2072. [CrossRef]
17. Dragomiretskiy, K.; Zosso, D. Variational mode decomposition. *IEEE Trans. Signal Process.* **2013**, *62*, 531–544. [CrossRef]
18. Zhang, M.; Xu, F. Variational mode decomposition based modal parameter identification in civil engineering. *Front. Struct. Civ. Eng.* **2019**, *13*, 1082–1094. [CrossRef]
19. Battula, V.V.R.; Krishna Rao, P.; Kantamaneni, S. Comparison of advanced signal decomposition techniques for the classification of PQDs by machine learning algorithms. *Sci. Rep.* **2025**, *15*, 38164. [CrossRef] [PubMed]
20. Li, N.; Wang, H. Variable filtered-waveform variational mode decomposition and its application in rolling bearing fault feature extraction. *Entropy* **2025**, *27*, 277. [CrossRef] [PubMed]
21. Shen, X.; Li, R. BroadBand-Adaptive VMD with Flattest Response. *Mathematics* **2023**, *11*, 1858. [CrossRef]
22. Ur Rehman, N.; Aftab, H. Multivariate variational mode decomposition. *IEEE Trans. Signal Process.* **2019**, *67*, 6039–6052. [CrossRef]
23. Mirjalili, S.; Lewis, A. The whale optimization algorithm. *Adv. Eng. Softw.* **2016**, *95*, 51–67. [CrossRef]

24. Wei, J.; Gu, Y.; Xie, Z.; Yan, Y.; Lu, B.; Li, Z.; Cheong, N.; Zhang, J.; Zhang, S. LSWOA: An enhanced whale optimization algorithm with Levy flight and Spiral flight for numerical and engineering design optimization problems. *PLoS ONE* **2025**, *20*, e0322058. [CrossRef] [PubMed]
25. Makhadmeh, S.N.; Kassaymeh, S.; Rjoub, G.; Bataineh, B.; Sanjalawe, Y.; Al-Betar, M.A. Recent advances in multi-objective whale optimization algorithm, its versions and applications. *J. King Saud. Univ. Comput. Inf. Sci.* **2025**, *37*, 200. [CrossRef]
26. Zhou, Y.; Hao, Z. Multi-strategy improved whale optimization algorithm and its engineering applications. *Biomimetics* **2025**, *10*, 47. [CrossRef] [PubMed]
27. Chen, M.; Cheng, Q.; Feng, X.; Zhao, K.; Zhou, Y.; Xing, B.; Tang, S.; Wang, R.; Duan, J.; Wang, J.; et al. Optimized variational mode decomposition algorithm based on adaptive thresholding method and improved whale optimization algorithm for denoising magnetocardiography signal. *Biomed. Signal Process. Control* **2024**, *88*, 105681. [CrossRef]
28. Ma, Y.; Wang, X.; Meng, W. A reinforced whale optimization algorithm for solving mathematical optimization problems. *Biomimetics* **2024**, *9*, 576. [CrossRef] [PubMed]
29. Wang, K.; Ma, X.D.; Jiang, T.; Yu, Y.; Wang, J.; Zhao, X. Fractional-order Kalman filter for dynamic deformation monitoring of super high-rise buildings. *Beijing Surv. Mapp.* **2024**, *38*, 661–666.
30. Guo, F.; Zhang, X. Adaptive robust Kalman filtering for precise point positioning. *Meas. Sci. Technol.* **2014**, *25*, 105011. [CrossRef]
31. Gao, G.; Yi, Y.; Zhong, Y.; Liang, S.; Hu, G.; Gao, B. A robust Kalman filter based on kernel density estimation for system state estimation against measurement outliers. *IEEE Trans. Instrum. Meas.* **2025**, *74*, 1003812. [CrossRef]
32. Wu, J.; Jiang, J.; Tang, Y.; Liu, J. Gaussian–student's t mixture distribution-based robust kalman filter for global navigation satellite system/inertial navigation system/odometer data fusion. *Remote Sens.* **2024**, *16*, 4716. [CrossRef]
33. Qu, X.; Ding, X.; Xu, Y.L.; Yu, W. Real-time outlier detection in integrated GNSS and accelerometer structural health monitoring systems based on a robust multi-rate Kalman filter. *J. Geod.* **2023**, *97*, 38. [CrossRef]
34. Shiri, H.; Wodecki, J.; Zimroz, R. Robust switching Kalman filter for diagnostics of long-term condition monitoring data in the presence of non-Gaussian noise. In *IOP Conference Series: Earth and Environmental Science*; IOP Publishing: Bristol, UK, 2023; Volume 1189, p. 012007.
35. Ma, C.; Pan, S.; Gao, W.; Liu, L. An improved multiple-outlier-robust kalman filter for GNSS/INS tightly coupled positioning in urban canyons. *IEEE Internet Things J.* **2025**, *12*, 48131–48145. [CrossRef]
36. Zeng, J.; Shi, Y.; Dai, K.; Liao, G. Real-time Structural displacement estimation by fusing acceleration and displacement data with adaptive kalman filter. *Adv. Eng. Sci.* **2023**, *55*, 188–196.
37. Smyth, A.; Wu, M. Multi-rate Kalman filtering for the data fusion of displacement and acceleration response measurements in dynamic system monitoring. *Mech. Syst. Signal Process.* **2007**, *21*, 706–723. [CrossRef]
38. Wu, J.; Jiang, J.; Zhang, C.; Li, Y.; Yan, P.; Meng, X. A novel optimal robust adaptive scheme for accurate GNSS RTK/INS tightly coupled integration in urban environments. *Remote Sens.* **2023**, *15*, 3725. [CrossRef]
39. Peng, Z.; Yu, J.; Meng, X.; Xie, Y.; Xie, Y. Dynamic parameters identification of long-span suspension bridges using enhanced VMD-SVD techniques with GNSS data. *Measurement* **2025**, *254*, 117914. [CrossRef]
40. Liu, X.; Han, H.; Wang, J.; Hancock, C.; Smith, A.; Yu, H. A GNSS/accelerometer integrated deformation monitoring model using fractional Kalman filtering. *Meas. Sci. Technol.* **2026**, *37*, 126302. [CrossRef]
41. Xiao, X.; Han, H.; Wang, J.; Li, D.; Chen, C.; Wang, L. Dynamic Deformation Analysis of Super High-Rise Buildings Based on GNSS and Accelerometer Fusion. *Sensors* **2025**, *25*, 2659. [CrossRef] [PubMed]
42. Xie, Y.; Zhang, S.; Meng, X.; Nguyen, D.T.; Ye, G.; Li, H. An innovative sensor integrated with GNSS and accelerometer for bridge health monitoring. *Remote Sens.* **2024**, *16*, 607. [CrossRef]
43. Ji, X.; Ren, L.; Fu, X.; Zhang, Q.; Li, H. Deformation monitoring of monopole communication towers based on multi-source data fusion. *Buildings* **2023**, *13*, 2709. [CrossRef]
44. *GB 50026-2020*; Standard for Engineering Surveying. China Planning Press: Beijing, China, 2020.
45. *JGJ 8-2016*; Technical Code for Deformation Measurement of Buildings and Structures. China Architecture & Building Press: Beijing, China, 2016.

Disclaimer/Publisher's Note: The statements, opinions and data contained in all publications are solely those of the individual author(s) and contributor(s) and not of MDPI and/or the editor(s). MDPI and/or the editor(s) disclaim responsibility for any injury to people or property resulting from any ideas, methods, instructions or products referred to in the content.